# Assessment of MicroInductors for DC-DC Converters

**Conference Paper** · January 2007

DOI: 10.1109/EMAP.2006.4430641 · Source: IEEE Xplore



**4 authors:**

D. Flynn
Heriot-Watt University


Hua Lu
University of Greenwich


Chris john Bailey
University of Greenwich


M.P.Y. Desmulliez
Heriot-Watt University

# Assessment of MicroInductors for DC-DC Converters

David Flynn†, Hua Lu‡#, Chris Bailey‡ and Marc Desmulliez†
†MicroSystems Engineering Centre (MISEC), Heriot-Watt University,
Riccarton EH14 4AS, Scotland, UK
‡School of Computing and Mathematical Sciences, University of Greenwich,
30 Park Row, London SE10 9LS, UK
#Email: h.lu@gre.ac.uk, Telephone: +442083318536

## Abstract

There are increasing demands on the power density and efficiency of DC-DC power converters due to the soaring functionality and operational longevity required for today's electronic products. In addition, DC-DC converters are required to operate at new elevated frequencies in the MHz frequency regime. Typical ferrite cores, whose useable flux density falls drastically at these frequencies, have to be replaced and a method of producing compact component windings developed. In this study, two types of microinductors, pot-core and solenoid, for DC-DC converter applications have been analyzed for their performance in the MHz frequency range. The inductors were manufactured using an adapted UV-LIGA process and included electrodeposited nickel-iron and the commercial alloy Vitrovac 6025 as core materials. Using a vibrating sample magnetometer (VSM) and a Hewlett Packard 4192A LF-impedance analyzer, the inductor characteristics such as power density, efficiency, inductance and Q-factor were recorded. Experimental, finite element and analytical results were used to assess the suitability of the magnetic materials and component geometries for low MHz operation.

## Introduction

Switching mode power conversion and management circuits can be found in most electronic devices. Fundamental to the operation of many of these circuits are the magnetic components, such as inductors and transformers. Typically, the magnetic components are the largest component on the PCB. With increasing frequency the size of the passive components can be reduced, hence, in partnership with improved switching technology, switching frequencies of DC-DC converters have been pushed into the range of 0.5 MHz-10 MHz [1-4].

Along with the increase in frequency and reduction in component size, novel manufacturing and packaging methods using alternative magnetic materials have also become desirable and feasible. At present, most magnetic components still utilize traditional ferrite cores with wire-wound or planar windings. Recently, magnetic components employing commercial or electrodeposited thin film magnetic alloys and windings fabricated via UV-photolithography have become viable alternatives. In the mega Hertz frequency range eddy currents in the magnetic core are important issues and in order to achieve high efficiency good understanding of the loss mechanisms and clear design rules are needed to ensure efficient designs.

The efficiency of DC-DC power converters operating in the mega Hertz frequency regime will depend heavily on the performance of the magnetic components. Ferrite cores, the present material of choice, suffers from a reduction in useable flux density at these elevated frequencies, and their high temperature sinter manufacture makes them non-compatible with neighboring components, preventing further integration. Hence, an alternative core material is sought and the ability to produce highly compact component windings desired. New core materials must have high resistivity, high saturation flux, relative permeability of 100-3000 and low coercivity. Moreover, these materials must be suitable for thin film deposition such that core losses can be minimized. The development of cost-effective mass-manufacturing of these thin films will also be a high priority.

Previous attempts to develop microscale magnetic components utilizing thin film alloys have demonstrated improvements in device performance. However, these development efforts have suffered from either slow or expensive deposition of the magnetic alloy [5], limited bandwidth of operation due to film thickness, and high relative permeability [6] or low saturation flux density [7]. Electrodeposition of magnetic alloys is a fast and economical thin film fabrication process. Also, during deposition magnetic properties may be tailored via waveform parameters, magnetic field annealing or bath composition. Complications of fabricating sufficient core cross sectional area from thin laminate can be overcome through careful design of the core structure. For example, utilizing vertical as opposed to horizontal laminate, or applying air insulation layer via sacrificial layer removal [8, 9]. Therefore, electrodeposition is considered as the preferred method of magnetic alloy deposition.

The focus of this paper is to analyze the performance of electrodeposited nickel-iron and cobalt based commercial alloy Vitrovac as potential core materials within inductors for the mega Hertz frequency range. In the following sections, the micro-inductor design and fabrication process will be described. This will then be followed by the characterization of the magnetic core materials and the experimental measurements and assessment of the performance of the prototype inductors. Then, a finite element computer modeling method will be described as a tool for the design and analysis of microinductors.

## Inductor Design and Fabrication Process

Pot-core and solenoid inductor designs are used in this research but other types of inductor designs such as the spiral and meander are also used in applications and research [5]. A single layer solenoid component allows near ideal performance [13]. The number of turns per single layer of traditionally wound solenoid inductors is limited by the core's inner diameter and how tightly you can pack the turns together. To increase inductance, a larger core or multiple

1-4244-0834-2/06/$20.00 ©2006 IEEE

layers of windings would normally be needed. This would lead to an increase in component size and parasitic capacitance. UV-photolithography discussed within the manufacturing of the solenoid allows a higher winding density. The solenoid also permits the inclusion of the core prior to interconnecting the lower and upper layers of the windings, therefore, is useful as a test vehicle for multiple materials.

The pot-core component is relatively easy to design, analyze and manufacture. Examples of the inductors used in this work are shown in Figures 1 and 2.

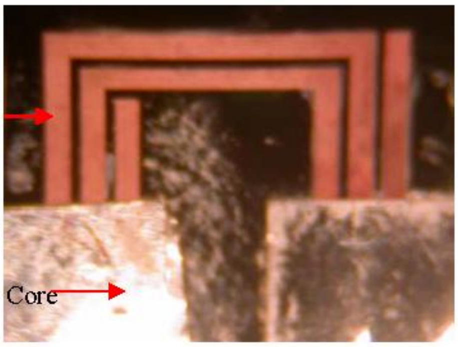


Figure 1. A Pot-Core 3-turn micro-inductor.

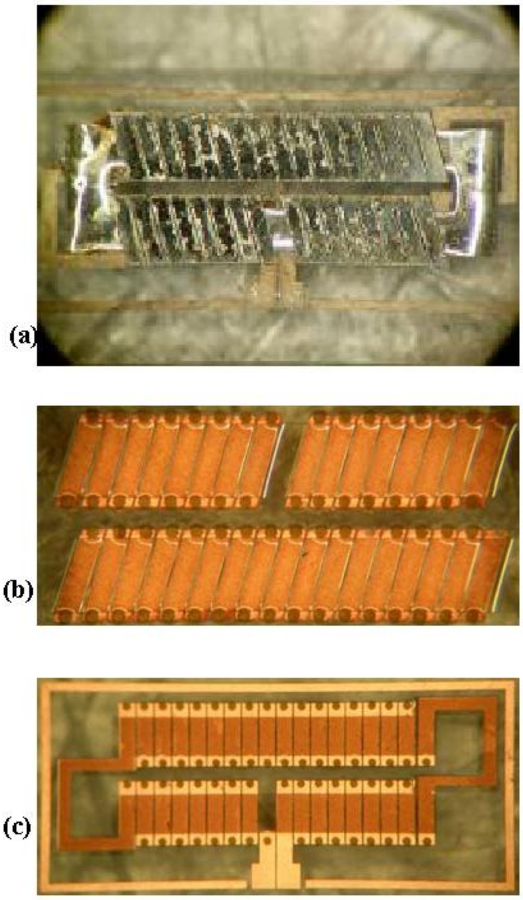


Figure 2. (a) A fabricated solenoid micro-inductor. (b) The upper winding and (c) the lower winding of the inductor.

A summary of the solenoid inductor fabrication process is given below:

**Step 1** A 3 inch glass wafer is immersed in deionized water and cleaned for 3 hours within an ultrasonic bath.

**Step 2** A 100-200nm thick titanium adhesion layer is deposited using electron beam evaporation followed by 100-200nm thick layer of nickel.

**Step 3** A positive photoresist AZ 9260 is deposited to obtain the required conductor and core thickness.

**Step 4** AZ 9260 is patterned with UV light, using an acetate mask in a contact exposure mode. Energy dose of approximately 2000mJ for 90μm thick resist is carried out and followed by 5 minutes of development immersed in a dilute 1:3 developer:deionised water.

**Step 5** The upper and lower winding layers are DC electroplated either Cu or Ni, 90μm thick. With the use of multiple AZ resist layers or a thick film resist such as SU-8 thicker winding layers could have been fabricated [14-16].

**Step 6** AZ is re-deposited and patterned, and gold bumps are electroplated. AZ is stripped with acetone. The seed layer is etched and AZ insulation is deposited and patterned.

**Step 7** The magnetic core is electroplated and etched free.

**Step 8** The lower insulation layer is coated with a 5μm thick non-conductive adhesive layer. The core is placed on the adhesive layer and after 5 minutes is permanently fixed. The lower and upper winding layer bonded through thermocompression with a maximum temperature of 220°C and 40-60g/per bump of pressure. The temperature is lower than the Curie temperatures of the alloys investigated [17, 18].

**Step 9** Titanium etchant is used to release the glass substrate off the upper layer. The final solenoid component with 90μm thick windings has dimensions 5mm x 2.0mm x 0.25mm.

The pot-core inductors were made using similar fabrication processes as the solenoid. The winding structures are fabricated on Kapton polyamide film which has a bulk resistivity of about $2x10^{17}\ \Omega$/cm and the film thickness is 25μm. The windings are fabricated on Kapton for two reasons: to release the winding structure from the glass substrate and insulate the windings from the lower core layer. Upper layers of the magnetic core are then assembled by applying non-conductive adhesive on top of the winding structure. The 3-turn windings are fabricated with a 10mm x 15mm x 0.37mm (*w x l x h*) footprint. The single turn component simply uses a strip of conductive copper tape. When the commercial alloy 6025 was used for the inductor core it was secured to a wafer and patterned with AZ 9260 and wet etched to the desired dimensions using $HNO_3:HCl:H_2O$, 2:1:3. The dimensions of the pot-core and solenoid inductors are summarized in Table I and II.

Table I: Prototype pot-core inductor dimensions.

| **Dimensions** | **NiFe** | **Vitrovac** |
|---|---|---|
| Number of turns | 3 | 1 |
| Turn thickness(μm) | 30 | 65 |
| Turn width(μm) | 300 | 10000 |
| Turn spacing(μm) | 50 | --- |
| Number of Core laminations | 10 | 1 |
| Lamination thickness(μm) | 10 | 20 |
| Lamination width(mm) | 6 | 10 |
| Lamination insulation(μm) | ≈10 | ≈10 |

Table II: Prototype solenoid inductor dimensions.

| Dimensions | |
|---|---|
| Number of Turns | 33 |
| Turn Thickness | 90 μm |
| Turn Width | 200 μm |
| Turn Spacing | 20 μm |
| Number of laminations | 1 |
| Lamination width | 500 μm |
| Lamination thickness | 10-20 μm* |
| Lamination insulation | ≈10 μm |

(*Vitrovac 20μm film thickness and electrodeposited alloy 10 μm)

## Experimental Results

***Magnetic material characterization***

A Vibrating Sample Magnetometer (VSM) was used to obtain the magnetic properties such as the saturation flux density $B_{sat}$ , the maximum applied field $H_{sat}$ , the coercivity $H_c$ , the remanence $B_r$ and the permeability $\mu$ . The resistivity of the films was measured using the four-point probe method. Manufacturer data was utilized for the estimation of Vitrovac performance. A Hewlett Packard 4192A LF-impedance analyzer was then used to record the inductance, resistance and Q-factor of the inductors, over a frequency range of 1 kHz-10MHz. The parameters utilized in the theoretical calculations are contained in Table III.

Table III: Electrical and magnetic material properties of the magnetic cores.

| Material | $\rho$ (μΩ.cm²) | $B_{sat}$ (T) | $H_c$ (Oe) | $\mu_r$ | Film height (μm) |
|---|---|---|---|---|---|
| Vitrovac | 130 | 0.5 | 0.05 | 100000 | 20 |
| NiFe | 20 | 0.8 | 3 | 2000 | 10 |

***Pot-core inductors results***

The total inductance of the device consists of the main inductance attributed to the core, $L_{AC}$ , in series with the intrinsic and leakage inductance of the windings. Leakage and intrinsic inductance of the windings is negligible in comparison to the main inductance of the core. A closed magnetic core utilizing high relative permeability material will confine the majority of the flux within the core. This was validated with an ANSYS simulation [11].

The measured $L_{AC}$ changes as a function of frequency. Equation (1) models the varying inductance of the core, the main inductance, with frequency;

$$L_{AC} = L_{DC}\,\frac{1}{\dfrac{b}{\delta}} \times \frac{\sinh\left(\dfrac{b}{\delta}\right) + \sin\left(\dfrac{b}{\delta}\right)}{\cosh\left(\dfrac{b}{\delta}\right) + \cos\left(\dfrac{b}{\delta}\right)} \qquad (1)$$

Where $L_{DC}$ , $\delta$ and $b$ are the DC inductance, the skin depth and the core thickness respectively [12].

The Q-factor of the component, which expresses the ratio of stored to dissipated power, is expressed as:

$$Q = \frac{\omega L_{AC}}{R_{tot}} \qquad (2)$$

where $\omega$ , and $R_{tot}$ are the radian frequency and the total resistance. respectively. The theoretical and modeled inductance, $L_{AC}$ , and $Q$-factors for the 3-turn and the 1-turn inductors are shown in Figures 3, 4, 5 and 6, respectively.

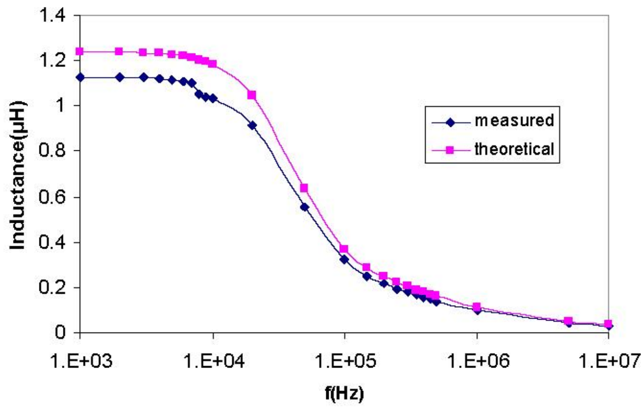


Figure 3. The inductance vs. Frequency for the 1-turn inductor with Vitrovac core.

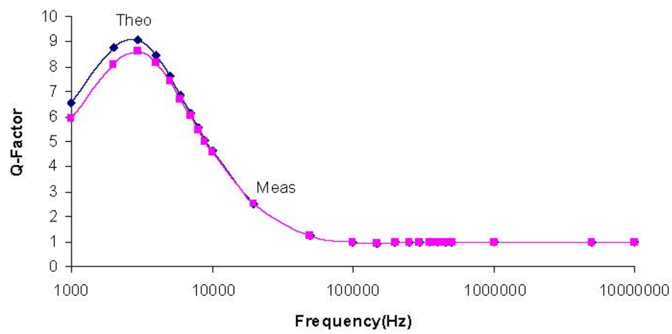


Figure 4. Q-factor vs. Frequency for the 1-turn inductor with Vitrovac core.

The variation between measured and theoretical results is attributed to a variety of factors such as the influence of the air-gaps introduced by the Kapton film and adhesive layers. Also, stresses induced in the magnetic film during assembly may affect the relative permeability of the film.

The results within Figures 3 & 5 indicate that as frequency increases the inductance decreases. The reduction in inductance is the result the domains within the alloy not rotating as freely at increased frequency and the cancellation flux due to eddy currents. The Vitrovac alloy exhibits this reduction at about 10 kHz but for the NiFe alloy, this effect occurs at approximately 0.5 MHz. Due to the high relative permeability of Vitrovac and film thickness of 20μm, it is assumed that cancellation flux produced by induced eddy currents is the main source of this phenomenon.

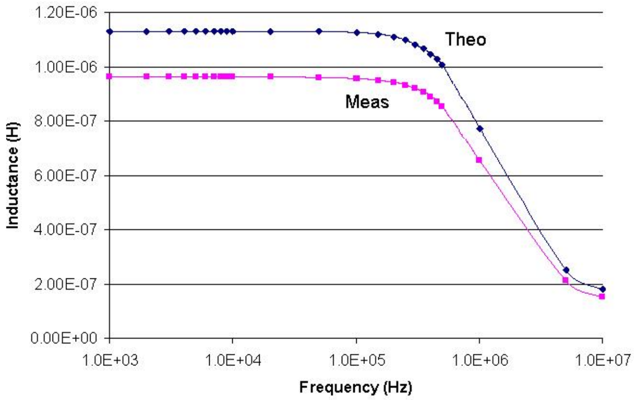


Figure 5. Inductance vs. frequency for the 3-turn pot-core inductor with NiFe alloy.

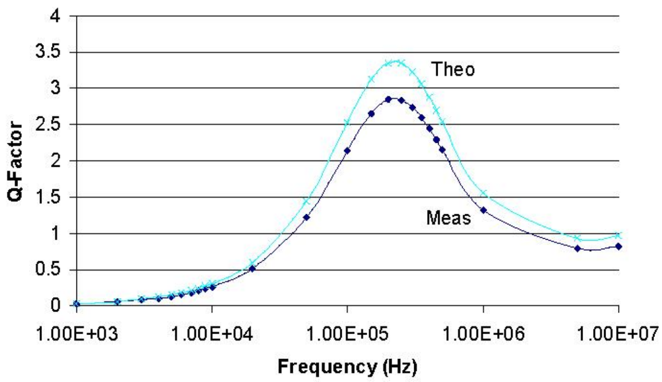


Figure 6. Q-factor vs. frequency for the 3-turn pot-core inductor with NiFe core.

As shown in Figure 4 & 6, the Q-factor peak for the NiFe inductor is located at a higher frequency than the Vitrovac inductor. These results show that the electroplated alloy is more suitable for higher frequency operation. In order for Vitrovac to operate at frequencies greater than 1 MHz, the relative permeability must be reduced, film thickness reduced, resistivity increased and ideally larger saturation flux density, to permit larger current. A common method of achieving many of these objectives is to introduce air gaps into the core.

***Solenoid inductor results***

The behaviors of Vitrovac in the solenoid inductor are similar to those in the pot-core inductor. Figures 7 and 8 show that the inductance value decreases rapidly long before the frequency reaches 0.5 MHz for the Vitrovac while for electroplated NiFe this happens when the core thickness equals approximately one skin depth, occurring just below 1 MHz.

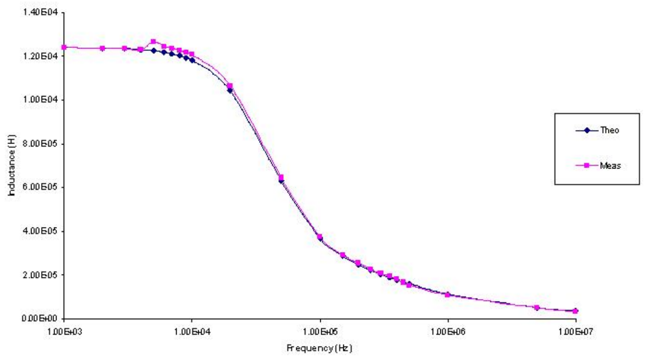


Figure 7. Vitrovac solenoid inductor inductance vs. frequency..

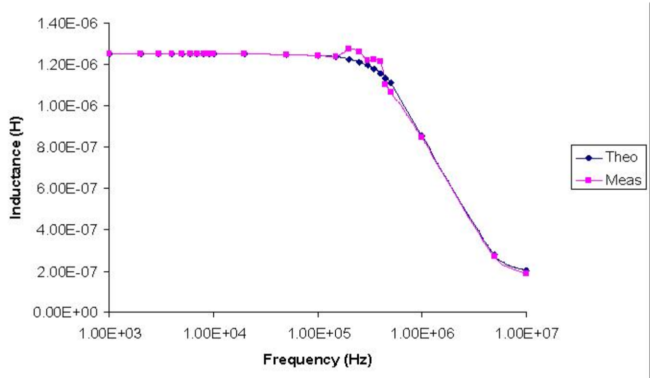


Figure 8. NiFe solenoid inductor inductance vs. frequency.

***Power density and efficiency of Solenoid inductors***

The maximum power density and efficiency of an inductor are essential parameters in inductor designs. The factors that affect these characteristics are the saturation flux density, the geometry of the core, the waveform, the resistivity of the core and the number and dimension of the windings etc.

The maximum power output can be achieved by setting the current just below the saturation value:

$$I_{sat} = \frac{B_{sat} \Re A_c}{N} \tag{5}$$

where $B_{sat}$, $\Re$, $A_c$ and $N$ is the flux density at which the magnetic core saturates, reluctance of the core, core cross sectional area and number of winding turns, respectively. With the value of saturation current known, and for a fixed value of the current density (10A/mm$^2$ typically for a printed circuit board), the winding cross-sectional area can be calculated in order to handle the saturation current.

The skin effect and proximity effect losses in the windings can be described by an AC resistance $R_{AC}$ determined by multiplying the DC resistance $R_{DC}$ by a factor $F_r$, which can be approximated by;

$$F_r = 1 + \frac{5p^2 - 1}{45}\varphi^4 \tag{6}$$

where $p$ is the number of winding layers and $\varphi$ is the ratio of conductor thickness to skin depth [19]. To minimize $R_{AC}$ the width of the individual turns, $W_t$, is adjusted to minimize the resistance factor, $F_r{'}$, that takes into account the reduction in conductor area due to spacing between windings;

$$F_r{'} = F_r \frac{W_t + S_t}{W_t} \quad (7)$$

$$R_{AC} = F_r{'} R_{dc} \quad (8)$$

$$R_{DC} = \rho \frac{l}{A_w} \quad (9)$$

where $S_t$ is the spacing between turns, $l$ is the length of the windings, $A_w$ is the winding cross sectional area and $\rho$ is the resisitivity of the winding material. At 1 MHz for a copper winding with inter-winding spacing of 20μm, an optimal width of 200μm is determined for a 90μm thick winding. The 4.5:1 aspect ratio is well within the limitations of the photoresist AZ9260 used in the manufacture of the component.

The output power of the inductor is defined as $P_{out} = V_{out} \times I_{out}$ where $V_{out}$ and $I_{out}$ are the voltage and current of the inductor respectively.

In order to determine the efficiency of the device the dissipation of power due to core loss and winding loss needed to be calculated. The power loss due to eddy currents, $P_{eddy}$, and hysteresis, $P_{hys}$, within the core can then be calculated [17]. The sum of these two terms forms the power loss of the core, $P_{core}$. Through the calculated winding resistance and known applied current, the power loss due to the windings, $P_{Cu}$, can be found using the Joules' law $P_{Cu} = I^2 R_{AC}$.

The overall efficiency, $\eta$, of the microinductor is then given by:

$$\eta = \frac{P_{out}}{\left(P_{out} + P_{core} + P_{Cu}\right)} \quad (10)$$

The efficiency and the power density for Vitrovac and NiFe solenoid components operating at 250 kHz and 500 kHz are listed in Table III.

The performance of the pot-core components in terms of power density and efficiency is summarised in Table IV. The magnetic core area is far greater in comparison to the solenoid component; as a result the eddy current loss is even more detrimental to component performance. The eddy current loss is calculated per laminate layer, then multiplied for the total number of laminate, then multiplied by two due to the pot-core symmetry.

The Vitrovac core is not suitable for the assessed frequencies. The low saturation current as a result of the low flux density and very high relative permeability, results in a low output power that is less than the dissipated eddy current power loss. Therefore, the material cannot be used within the solenoid micro-inductor for operation in the selected frequency range.

Table III: Solenoid Power Density and Efficiency at 250 kHz and 500 kHz.

| 250kHz | | |
|---|---|---|
| Parameters | NiFe | Vitrovac |
| $I_{out}$ (mA) | 100 | 1.32 |
| $L$ (μH) | 1.25 | 22 |
| $V_{out}$ (V) | 0.146 | 0.183 |
| $P_{out}$ (mW) | 14.6 | 0.24 |
| $P_{eddy}$ (mW) | 1.80 | 0.8 |
| $P_{hys}$ (mW) | 0.09 | 0.01 |
| $P_{cu}$ (mW) | 0.5 | 0.00008 |
| Efficiency (%) | 85 | X |
| Power Density (W/cm³) | 5 | X |
| **500kHz** | | |
| Parameter | NiFe | Vitrovac |
| $I_{out}$ (mA) | 100 | 1.32 |
| $L$ (μH) | 1.07 | 15.5 |
| $V_{out}$ (V) | 0.29 | 0.36 |
| $P_{out}$ (mW) | 29 | 0.47 |
| $P_{eddy}$ (mW) | 7.23 | 3.47 |
| $P_{hys}$ (mW) | 0.198 | 0.02 |
| $P_{cu}$ (mW) | 0.5 | 0.00008 |
| Efficiency (%) | 78 | X |
| Power Density(W/cm³) | 9 | X |

Table IV: 3-turn and 1-turn Micro-inductor performance at 50 kHz for NiFe and Vitrovac core materials.

| Parameter | NiFe 3-turn | Vitrovac 1-turn |
|---|---|---|
| $I_{out}$ (mA) | 90 | 79 |
| $L$ (μH) | 0.96 | 1.25 |
| $V_{out}$ (V) | 0.31 | 0.02 |
| $P_{out}$ (mW) | 27.9 | 1.75 |
| $P_{eddy}$ (mW) | 15.79 | 2.53 |
| $P_{hys}$ (mW) | 4.32 | 0.018 |
| $P_{cu}$ (mW) | 1.88 | 0.006 |
| **Efficiency** (%) | 55 | X |
| **Power Density** (W/cm³) | 0.27 | X |

In order to improve the power density of the Vitrovac inductor, the key is to increase the saturation current. One possible solution is to etch the Vitrovac film to form air gaps. For the NiFe inductor, the efficiency is not low but it can be improved by optimizing the number of laminations and the winding cross-section areas. The NiFe sample when transferring from 250 kHz to 500 kHz reduces in efficiency from 85 to 78%, but there is an increase in power density from 5 to 9W/cc. Clearly there is a trade-off between efficiency and power density. Also, at both frequencies eddy current power loss is the main loss mechanism and increases with frequency.

At 50 kHz the pot-core components operate inefficiently due to large eddy current loss. The performance of these components highlight the typical challenges encountered when trying to apply thin film magnetic alloys to power magnetic components. Improvements in performance would require thinner laminate and reduced core area. However, as the assembly process was manual this was not attempted. Sputtering would be a suitable process for such a component; however delamination and sidewall coverage would be a problem. Sullivan et al partially melted photoresist posts to create a slant to allow closure of lower and upper core layers [20]. Repeatability and temperature effects on the alloy could be recurrent problems.

### Computer Modeling of Micro-inductors

Finite Element (FE) computer modeling method has also been used in this study to predict the magnetic field, the eddy current, and inductance in the pot-core and solenoid inductors using the software package ANSYS®. The modeling results can be used to augment experimental results in the understanding of the loss mechanisms and in predicting the changes in the inductor performance when inductor structure and/or material properties have changed. This kind of virtual experiments can greatly reduce the time and financial burden in the inductor design process.

The pot-core model is a 2D model using the ANSYS PLANE13 elements with current density vector perpendicular to the plane. Since the the magnetic flux of a pot-core inductor is not completely confined to the core some air surrounding the inductor has to be included in the model. Figure 9 shows the schematic representation of the computer model. Symmetry of the inductor is used so that only ¼ of the inductor cross-section is included in the model. Figure 10 shows a model with two air gaps.

The solenoid model is a 3D model slice model using the ANSYS SOLID117 elements. Along the thickness there is only one layer of elements the model is in effect 2D in nature with the current density vectors parallel to the plane. Figure 11 shows the solenoid model. The current is fed at a boundary surface. The magnetic flux is perpendicular to the slice plane and no stray fields exist outside the inductor.

The key output parameters of the inductor models are the inductance, the losses, the resistance factor and the Q-factor. The method of obtaining these parameters can be found in [10, 11]. The modeled results and the experimental results for the solenoid inductor are consistent [11]. Figure 12 shows a comparison between the modeled and the measured inductance values.

For the 1-turn pot-core inductor the computer model presented in [10] is much smaller than the one described in this paper and it therefore has a much shorter magnetic path. This has to be taken into account when comparing the experimental results presented in this paper.

As it has been mentioned in previous sections, one way of making Vitrovac to work in the 1-10MHz frequency range is to introduce air gaps. The effects of these gaps were investigated in [10]. Results showed that with the introduction of ten 5-micron gaps the inductance decreased by about 50%. Results presented in [11] also showed that the peaks of the Q-factor vs. frequency curves become broader and shifted to the higher frequency end making the commercial more suitable for high frequency applications.

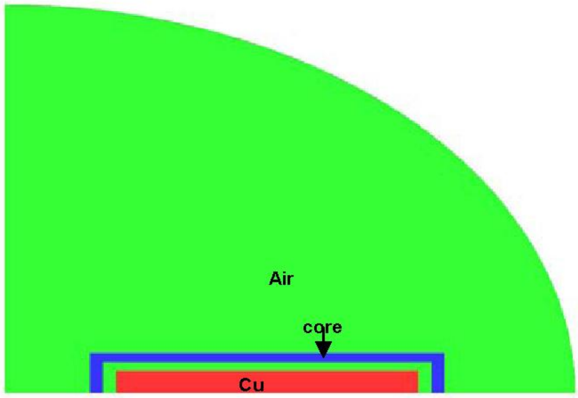


Figure 9. The ¼ model of the 1-turn inductor. The drawing is not to scale.

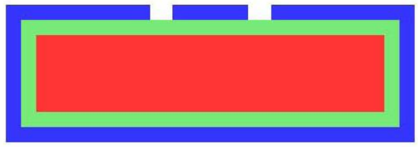

Figure 10. A model with two air gaps. A ½ model is used because of the symmetry.

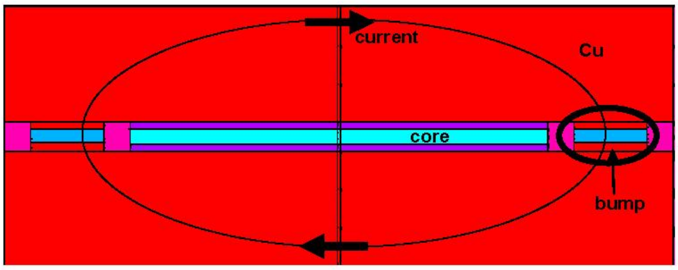


Figure 11. Schematic of a slice of the solenoid inductor. Only one quarter of it needs to be modeled because of the symmetry.

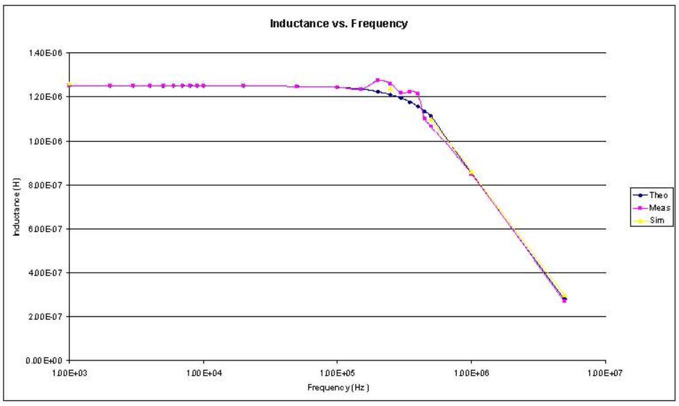


Figure 12: The measured and modeled values of the inductance for the solenoid inductor with 10μm NiFe core material in (a) and (b) respectively.

### Conclusions

The commercial magnetic alloy Vitrovac and electroplated NiFe laminates have been investigated for their potential use as the magnetic core materials of micro-inductors. Due to high relative permeability, inductors using Vitrovac can only operate in the low kHz frequency range. Computer modeling results show that by introducing air gaps this situation could be changed.

Electroplated NiFe laminates with a laminate thickness of 10 microns perform better than the commercial alloy in the frequency range of interest. In the case of the solenoid inductor the power density and efficiency of the NiFe alloy is superior. Currently, magnetic components are required to operate with efficiency in the high nineties; hence optimization of the component is required. The drawback of using the NiFe core, and similar soft magnetic alloys, is that more laminates are needed in order to achieve the desired inductance because of their low relative permeability. An increase in core area allows a larger current to be applied. Electrically and magnetically tailored materials utilizing mass production and novel fabrication processes to produce multiple thin laminate will provide the high power density magnetic components of the future. Novel manufacturing processes and materials are being investigated.

**Acknowledgments**

This work is supported by the Engineering and Physical Sciences Research Council (EPSRC) in the UK, Raytheon Systems Limited and the Institution of Engineering and Technology (IET).

**References**

1. Van Wyk, J.D. and Lee, F., “Power Electronics Technology at the Dawn of the New Millenium – Status and Future”, *Power Electronics Specialists Conference*, vol.1, 27 June 27 – July 1, 1999
2. Huljak, R.J., Thottuvelil, V.J., Marsh, A.J. and Miller, B.A, “Where are power supplies headed?”, *Applied Power Electronics Conference and Exposition*, 2000. APEC 2000. Fifteenth Annual IEEE, Volume 1, 6-10, Feb. 2000, pp10-17
3. International Technology Roadmap for Semiconductors 2001 Edition, System Drivers (ITRS)
4. Lotfi, A.W. and Wilkowski, M.A., “Issues and advances in high-frequency magnetics for switching power supplies”, *Proceedings of the IEEE*, Vol. 89, Issue 6, June 2001 pp833 - 845
5. Chong, H. Ahn, and Mark G. Allen, “Micromachined Planar Inductors on Silicon Wafers for MEMS Applications”, *IEEE Transactions on Industrial Electronics*, Vol. 45, No. 6, 886-876 (1998)
6. Ohnuma, S., Lee, H.J., Kobayashi, N., Fujimori, H. and T. Masumoto, “Co-Zr-O Nano-Granular Thin Films with Improved High Frequency Soft Magnetic Properties”, *IEEE Trans. Magnetics*, Vol. 37, No 4, pp.2251-2254( 2001)
7. Dezuari, Q., Gilbert, S.E., Belloy, E., Gijs, M.A.M., “High inductance planar transformers”, *Sensors and Actuators* 81 355-358 (2000)
8. Park, J. Y., Lagorce, L. K. and M.G. Allen, “Ferrite-based integrated planar inductors and transformers fabricated at low temperature”, *IEEE Trans. Magn.* 33 3322–5 (1997)
9. Matthias Ludwig, Maeve Duffy, Terence O’Donnell, Paul McCloskey, Sean Cian O’Mathuna, “Design study for ultra flat PCB integrated inductors for low power conversion applications”, *International Magnetics Conference* (INTERMAG), Boston, MA, 2003, pp. 3193-3195
10. Lu, H., Flynn, D., Bailey, C., Desmulliez, M., “Computer modeling of a micro-manufactured 1-turn inductor”, *2006 Conference On High Density Microsystem Design And Packaging And Component Failure Analysis* (HDP '06), Poceedings : pp.241-246 (2006)
11. Hua Lu, David Flynn, Chris Bailey and Marc Desmulliez, An Analysis of a Microfabricated Solenoid Inductor, 2006 Electronics Systemintegration Technology Conference (ESTC) Proceedings, p556- 561 (2006)
12. Marian, K., Kazimierczuk, Giuseppe Sancineto, Gabriele Grandi, Ugo Reggiani, Antonio Massarini, “High frequency Small-Signal Model of Ferrite Core Inductors”, *IEEE Trans. Magnetics.*, Vol. 35, No.5, pp. 4185-4189 (1999)
13. Mark Seitz and Michael Roeber M. Seitz et al, “Squeeze More Performance Out of Toroidal Inductors”, *Power Electronics Technology*, August 2005.
14. Brunet, M., O’Donnell, T., O’Brien, J., McCloskey, P., Ó Mathuna, S.C., “Thick photoresist development for the fabrication of high aspect ratio magnetic coils”, *J.Micromech. & Microeng.* 12, IoP, 2002.
15. Vettiger, P., Brugger, J., Despont, M., Lorenz, H., Fahrni, N. and Renaud, P., “High-aspect-ratio, ultrathick, negative-tone near-UV photoresist and its applications for MEMS”, *Sensors and Actuators*, A 64 (1998) pp. 33-39.
16. Lorenz, H., Despont, M., LaBianca, N.C., Renaud, P. and Vettiger, P., “SU-8 a low cost negative resist for MEMS,” *J. Michromech. Microeng.*, vol. 7, pp. 121–124, 1997.
17. Daniel, L. and Sullivan,C.R., “Design of microfabricated inductors”, *IEEE, Trans on Power Electronics*, Vol. 14, No. 4, July 1999.
18. Senseky, M.K., “Electromagnetic Generators for Portable Power Applications”, PhD Thesis, University of California, Berkeley, 2005.
19. William Gerard Hurley, Eugene Gath and John G. Breslin, “Optimizing the AC Resistance of Multilayer Transformer Windings with Arbitrary Current Waveforms”, *IEEE Trans. Power Electron.*, Vol. 15, No.2, pp. 369-376 (2000)
20. Sullivan, “Measured performance of a high power density Microfabricated transformer in a DC-DC converter”, *27th Annual IEEE Power Elecronics Specialists Conference* 1996, pp. 287-294